Generalized Lévy walks and the role of chemokines in migration of effector CD8$^+$ T cells: Supplementary Information

Tajie H. Harris[1], Edward J. Banigan[2], David A. Christian[1], Christoph Konradt[1], Elia D. Tait Wojno[1], Kazumi Norose[3], Emma H. Wilson[4], Beena John[1], Wolfgang Weninger[5], Andrew D. Luster[6], Andrea J. Liu[2], and Christopher A. Hunter[1]

[1] *Department of Pathobiology, School of Veterinary Medicine, University of Pennsylvania, 380 S. University Ave., Philadelphia, PA 19104, USA*
[2] *Department of Physics and Astronomy, School of Arts and Sciences, University of Pennsylvania, 209 S. 33rd St., Philadelphia, PA 19104, USA*
[3] *Department of Infection and Host Defense, Graduate School of Medicine, Chiba University 1-8-1, Inohana, Chuo-ku, Chiba, 260-8670, Japan*
[4] *Division of Biomedical Sciences, University of California-Riverside, Riverside, CA 92521, USA*
[5] *The Centenary Institute, Newtown, NSW 2042 and Discipline of Dermatology, Sydney Medical School, Sydney, NSW, Australia*
[6] *Center for Immunology and Inflammatory Diseases, Division of Rheumatology, Allergy and Immunology, Massachusetts General Hospital, Building 149, 13th Street, Room 8301, Charlestown, MA 02129, USA*

Supplementary Figures and Legends

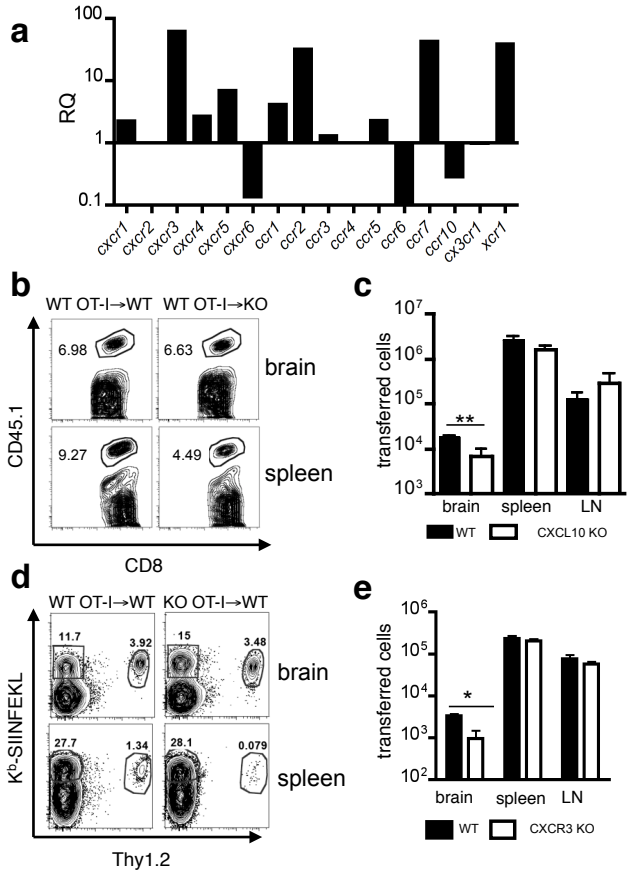

Supplementary Figure 1: CXCR3 expression is increased in the brain during chronic *T. gondii* infection and CXCR3/CXCL10 are required for optimal T cell trafficking to the CNS. (**a**) C57BL/6 mice were infected with 1×10^4 PruOVA parasites. RNA was isolated from whole brain tissue. Real time PCR specific for chemokine receptors and chemokines was performed and normalized to *hprt* mRNA. *In vitro* activated OT-I cells were transferred to mice infected with Pru^{OVA} parasites for 28 days. CD45.1-expressing OT-I cells were transferred i.v. into wildytype C57BL/6 (WT) or $\text{CXCL10}^{-/-}$ (KO) mice. After 7 days, transferred OT-I cells were identified by CD8 and CD45.1 expression by flow cyotmetry (**b**) and enumerated (mean ± SEM) in the brain, spleen, and cervical lymph nodes (LN) (**c**). Thy1.2^+ $\text{CXCR3}^{-/-}$ and WT OT-I cells were transferred to wildtype Thy1.1^+ recipients. Four days post-transfer, CD8^+, tetramer^+, and Thy1.2^+ cells were identified by flow cytometry (**d**) and enumerated (mean ± SEM) in the brain, spleen, and lymph node (**d**). $^*p < 0.05$, $^{**}p < 0.01$ by Students t-test. FACS plots are representative of three independent experiments with an n=4-5 per group.

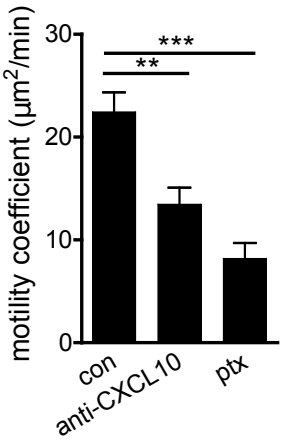

Supplementary Figure 2: The motility coefficient of $CD8^+$ T cells is reduced following anti-CXCL10 and pertussis toxin treatment. OT-I^{GFP} cells were expanded *in vitro* and transferred to mice chronically infected with Pru^{OVA} parasites. On day 7 post-transfer brains from mice that received PBS (con), 300 μg of anti-CXCL10 (anti-CXCL10), or 8 μg pertussis toxin (ptx) i.p. were imaged in 3 dimensions over 10 minutes. Volocity software was used to calculate the motility coefficient (displacement$^2/6t$). $^{**}p < 0.01$, $^{***}p < 0.001$ by one way ANOVA.

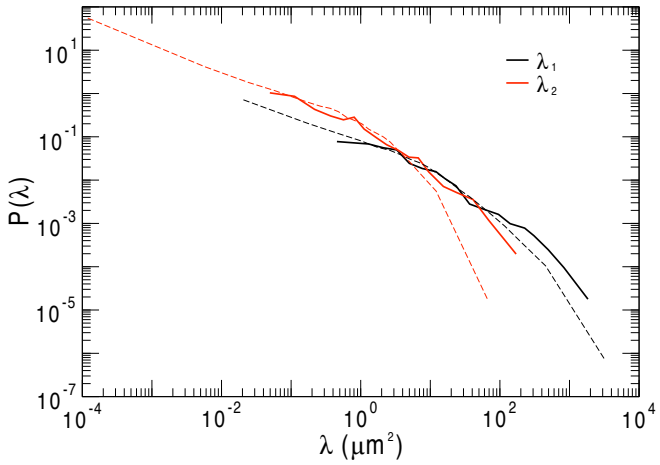

Supplementary Figure 3: Observed anisotropies in short-time cell motions are comparable to those of isotropic generalized Lévy walkers. We plot probability distribution of eigenvalues of the 2D moment of inertia tensors of cell trajectories for both control T cells (solid lines) and generalized Lévy walkers (dashed lines). The distribution of the larger eigenvalue, λ_1, is shown in black, and the distribution of the smaller eigenvalue, λ_2, is shown in red. Note that by model design, both the time and ensemble averages of generalized Lévy walk trajectories are isotropic. We find that the experimentally observed distributions of eigenvalues of the moment of inertia tensors compare favorably with those of the generalized Lévy walk model.

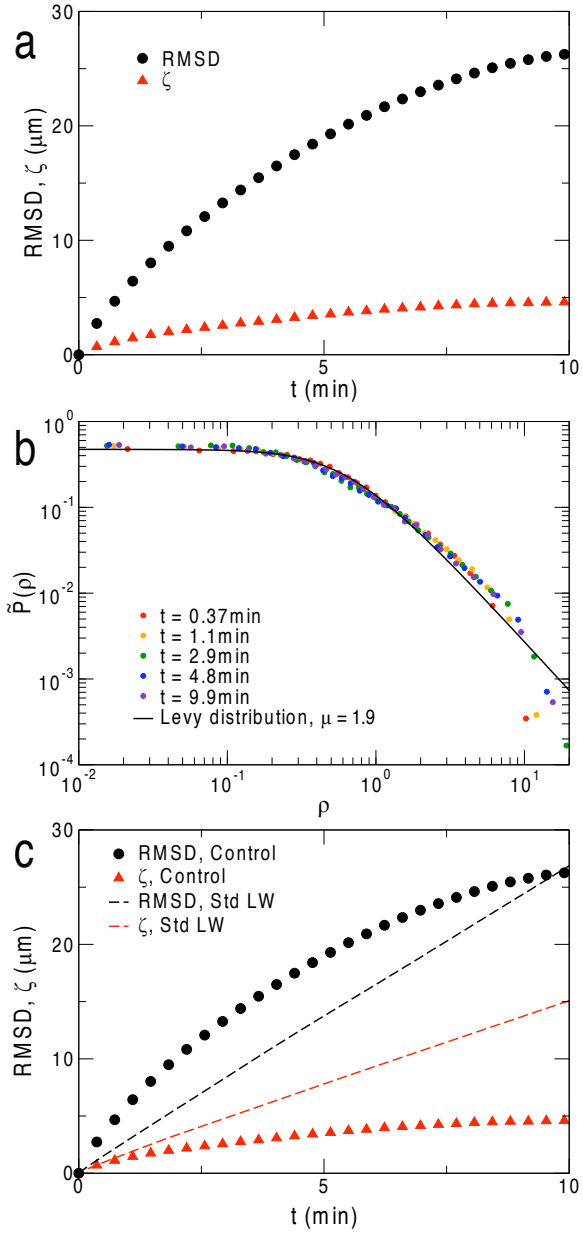

Supplementary Figure 4: Migrating T cells are not described by standard Lévy walks. a, The scale factor, ζ, is not the root-mean-squared displacement. For random-walk-like motility, the probability distribution of displacements would be Gaussian, with a scale factor, ζ, equal to the RMSD. For $CD8^+$ T cells in the brain, ζ (red triangles) is clearly distinct from the RMSD (black circles). **b,** Collapsed probability distributions of displacements (colored circles) appear to be well-described by a Lévy distribution with Lévy exponent $\mu = 1.9$ (black line). Although this is approximately what is expected for a standard Lévy walk with Lévy exponent $\mu = 1.9$, as shown in **c**, both the RMSD (black dashed line) and scale factor, ζ, (red dashed line) for a standard Lévy walk scale differently than the RMSD and ζ for the T cell probability distributions (black circles and red triangles, respectively). Specifically, for a standard Lévy walk with $\mu = 1.9$, the RMSD scales linearly in t (ballistic motion) and ζ scales as $t^{0.9}$, whereas in T cells, the RMSD grows as $t^{1.4}$ and ζ scales as $t^{0.63}$.

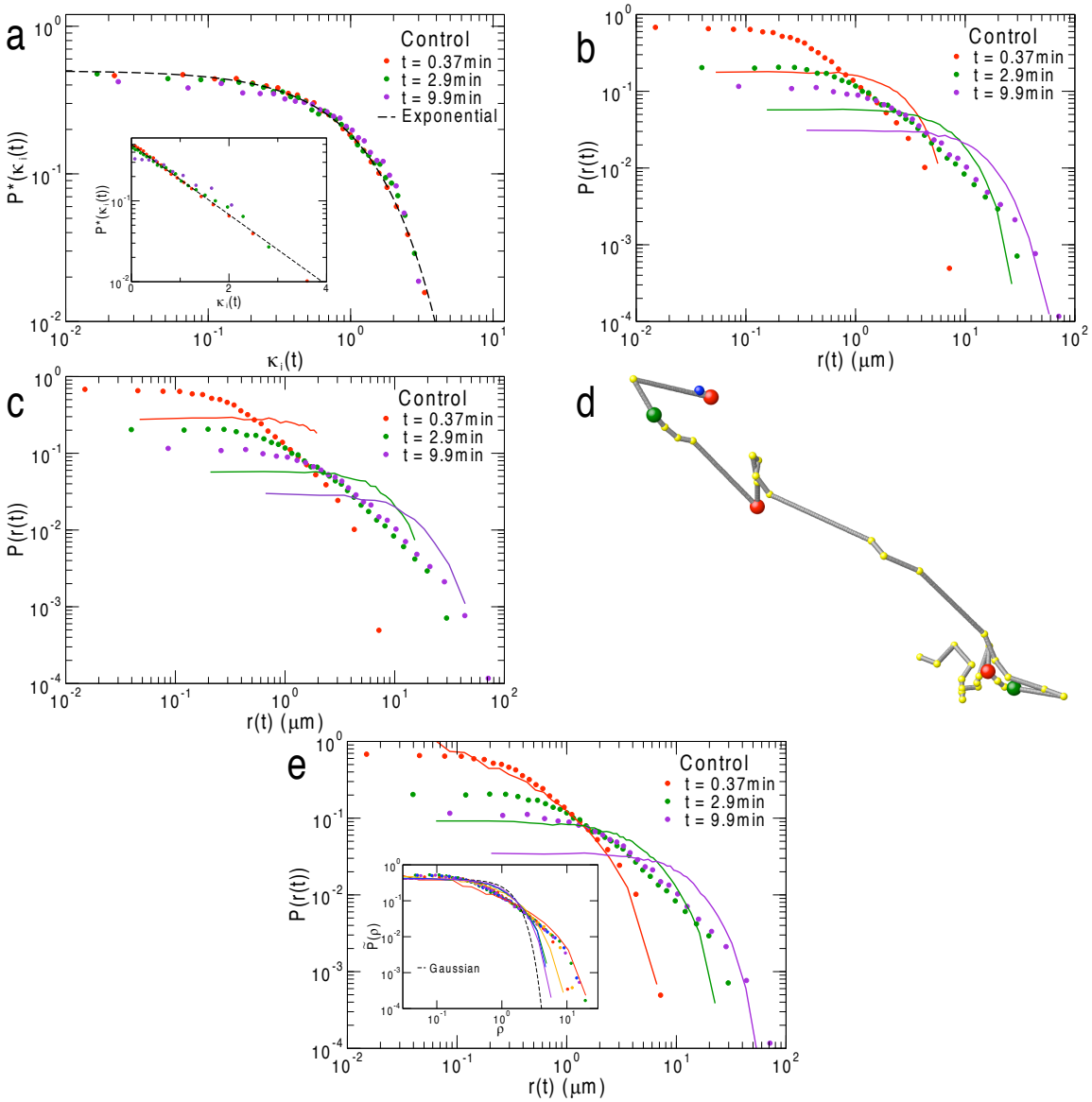

Supplementary Figure 5: Other random walk models do not reproduce the behavior of CD8$^+$ T cells in the brain. We attempted to **a-c**, fit models with walkers with exponentially-distributed run lengths and **d-e**, bimodal correlated random walkers (described in detail in refs. 25 and 61). **a**, In order to determine whether T cells execute generalized Lévy walks or collective Lévy behavior is due to variation from cell to cell, we plot the probability distributions, $P^*(\kappa_i(t))$, of scaled displacements, $\kappa_i(t) = r_i(t)/\bar{r}_i(t)$, as suggested by ref. 56. Scaled displacements, $\kappa_i(t)$, are the cell displacements, $r_i(t)$, for the i^{th} cell at various times divided by the mean displacement for that cell, $\bar{r}_i(t)$. For $t = 0.37$ min (red circles), $P^*(\kappa_i(t))$ appears to be exponential (dashed line), but for $t > 0.37$ min (green and purple circles), $P^*(\kappa_i(t))$ deviates from the unit exponential distribution. **Inset:** Although the early time distribution (red circles) appears to be a straight line on a semi-log plot for $t = 0.37$ min, $P^*(\kappa_i(t))$ deviates from this behavior for larger t (green and purple circles). **b-c**, To determine whether the observed migratory statistics of T cells could be obtained from an exponential model, we plotted the distribution, $P(r(t))$ of walker displacements using mean run lengths of cells after various times, t. As representative examples, in (**b**), we show the results of the model using mean run lengths of cells after $t = 0.37$ min and in (**c**), we show the results when we use mean run lengths after $t = 9.9$ min. In all tested cases, the model (colored lines) did not agree well with the experimental data (colored circles). **d**, The bimodal analysis[25,61] can identify starting points of directional (green) and reorientation (red) modes for bimodal correlated random walkers. However, this example of a cell track illustrates the failure of the bimodal analysis to accurately describe the behavior of CD8$^+$ T cells migrating in the brain. The blue sphere is the beginning of the cell track and the yellow spheres mark observed positions of the cell at various times. **e**, We compare probability distributions, $P(r(t))$, of T cells (colored circles) to those of simulated bimodal correlated random walkers (colored lines). The bimodal correlated random walk model does not agree with the observed behavior of T cells. **Inset:** Unlike the probability distributions of T cells (colored circles), the distributions of bimodal correlated random walkers (colored lines) do not collapse onto a single curve. In addition, the shapes of the displacement distributions appear to systematically approach a Gaussian distribution (dashed line).

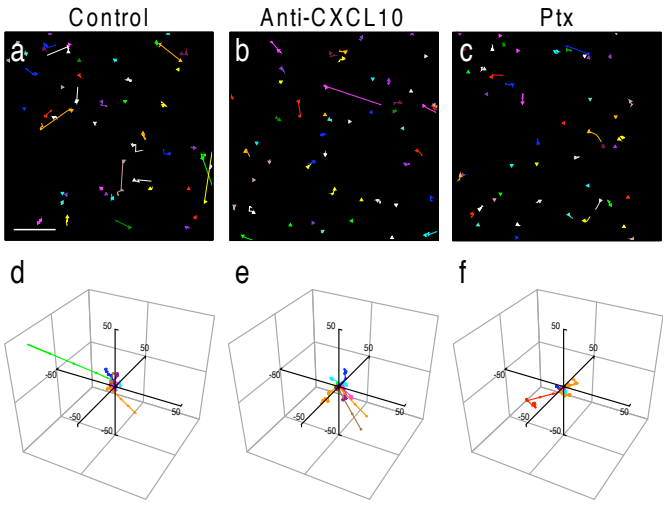

Supplementary Figure 6: Generalized Lévy fits for effects of chemokines on OT-I T cells in the central nervous system. Representative cell tracks from generalized Lévy walk model for control (**a**), anti-CXCL10-treated (**b**), and pertussis-toxin-treated systems (**c**) are shown in 2D (scale bar, 100 μm) projected into 2D, similar to Fig. 3 in the main text. **d-f,** 3D images of tracks from the generalized Lévy walk model visualized by plotting representative individual tracks from the origin for control (**d**), anti-CXCL10-treated (**e**), and pertussis-toxin-treated (**f**) systems.

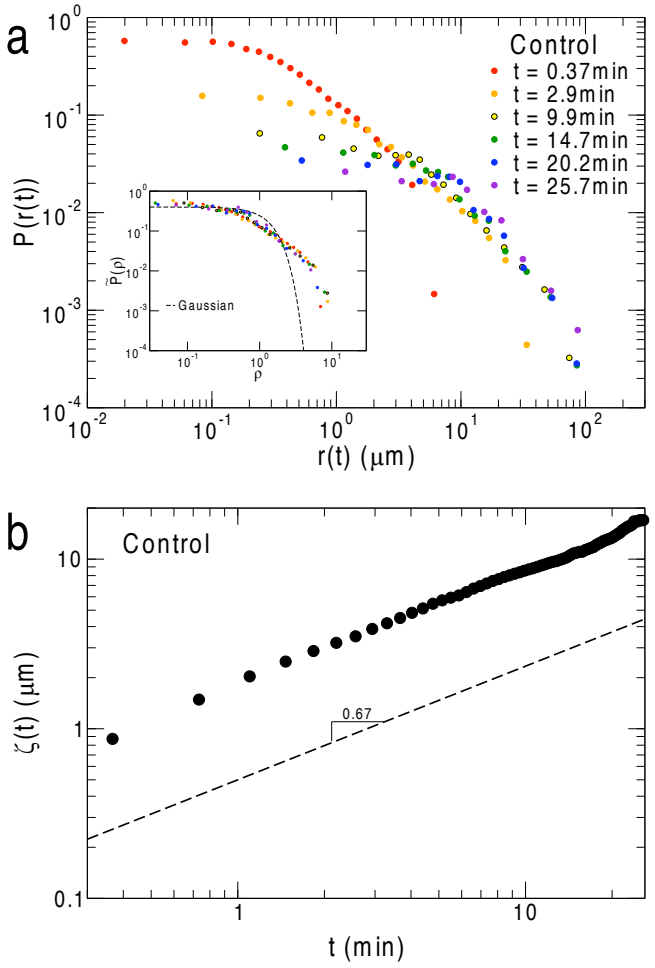

Supplementary Figure 7: Generalized Lévy walk behavior is observed in experiments lasting longer than 10 minutes. a, The shapes of displacement distributions, $P(r(t))$, at various times, t, of control cells is independent of time up to at least 25.7 min. **Inset:** By scaling displacements by a time-dependent scale factor, $\zeta(t)$, probability distributions collapse onto a single, non-Gaussian curve, $\tilde{P}(\rho)$, at all times up to at least 25.7 min. Displacement histograms have 800, 750, 575, 400, 250, and 125 displacements per bin for $t = 0.37, 2.9, 9.9, 14.7, 20.2,$ and 25.7 min, respectively. **b,** Consistent with Fig. 3c in the main text, the scale factor, ζ, grows approximately as a power law, t^{γ}, where $\gamma \approx 0.67$.

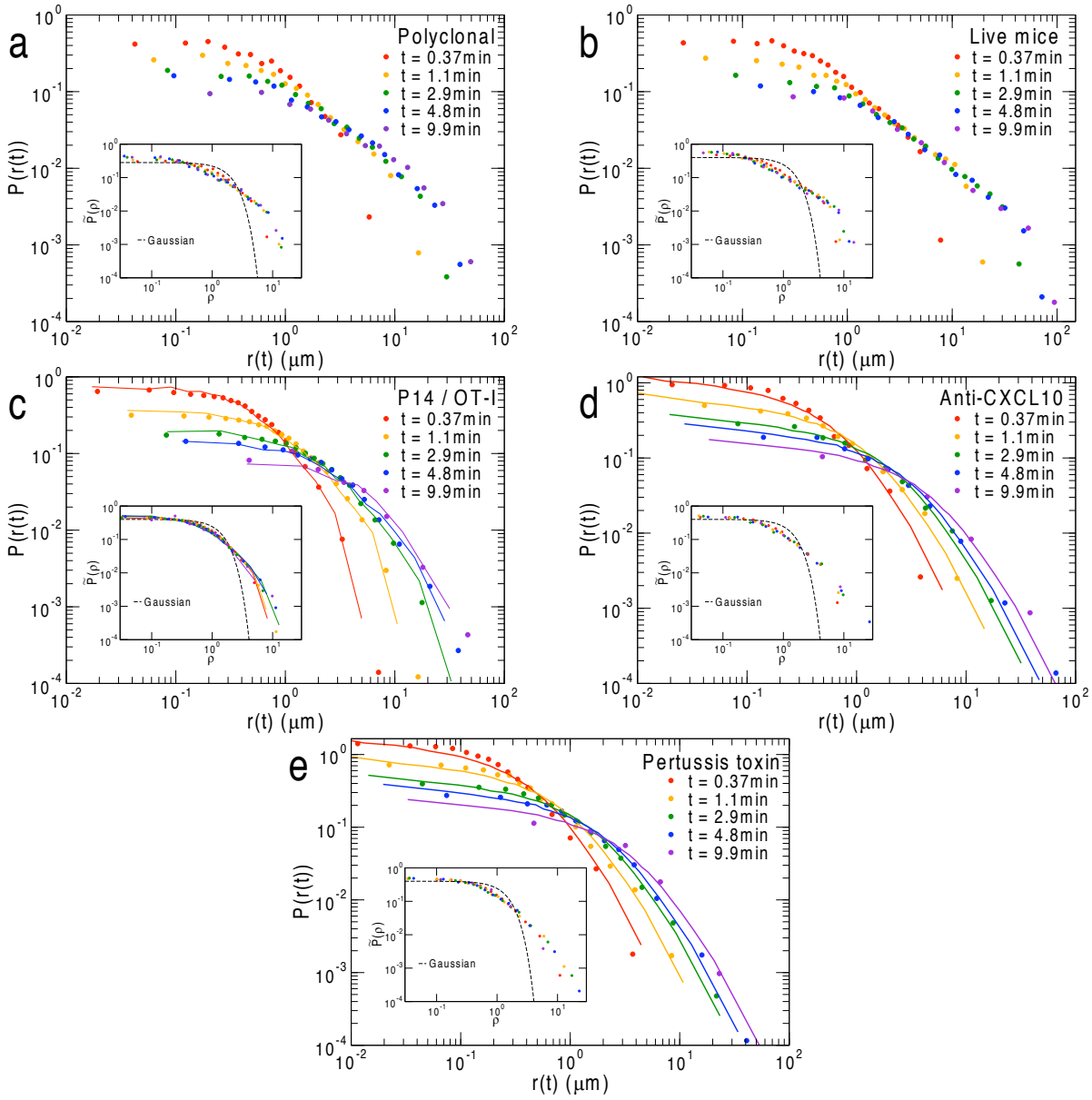

Supplementary Figure 8: Polyclonal and non-antigen-specific CD8$^+$ T cells, OT-I cells in live mice, and CD8$^+$ T cells in anti-CXCL10-treated and pertussis-toxin-treated mice migrate via generalized Lévy walks. a-e, The shapes of displacement distributions, $P(r(t))$, at various times, t, for (**a**) polyclonal T cells, (**b**) OT-I cells migrating in the brains of live mice infected with Pru$^{\mathrm{OVA}}$ strain parasites, (**c**, colored lines) OT-I T cells in mice infected with Pru$^{\mathrm{OVA}}$ strain parasites, (**c**, colored circles) P14 cells, specific for the gp33 protein of LCMV, in mice infected with Pru$^{\mathrm{OVA}}$ strain parasites, (**d**) CD8$^+$ T cells in anti-CXCL10-treated mice, and (**e**) CD8$^+$ T cells in pertussis-toxin-treated mice appear to be independent of t (colored circles). For ease of comparison in (**c**), OT-I T cell displacement distributions are shown as lines that connect individual data points which are not shown. CD8$^+$ T cells in both (**d**) anti-CXCL10- and (**e**) pertussis-toxin-treated cells are well described by the generalized Lévy walk model (colored lines). Histograms for polyclonal T cells contain 200, 185, 165, 150, and 140 displacements per bin for $t = 0.37, 1.1, 2.9, 4.8$, and 9.9 min, respectively. For histograms of OT-I T cell displacements in live mice infected with Pru$^{\mathrm{OVA}}$ strain, histograms contain 700, 650, 600, 550, and 300 data points per bin, respectively. For histograms of OT-I T cell displacements in mice infected with Pru$^{\mathrm{OVA}}$ strain, histograms contain 1000, 950, 900, 650, and 75 data points per bin, respectively. For P14 cells, histograms contain 1200, 1100, 1000, 850, and 90 data points per bin. Histograms for T cells in anti-CXCL10-treated mice contain 500, 480, 430, 335, and 40 displacements per bin, respectively. Histograms for T cells in pertussis-toxin-treated mice contain 800, 725, 660, 525, and 85 displacements per bin, respectively. **Insets:** In each case, probability distributions, $\tilde{P}(\rho)$, of rescaled displacements, ρ, at various times collapse onto a single curve (colored circles). These collapsed curves are clearly different from a Gaussian distribution (dashed line).

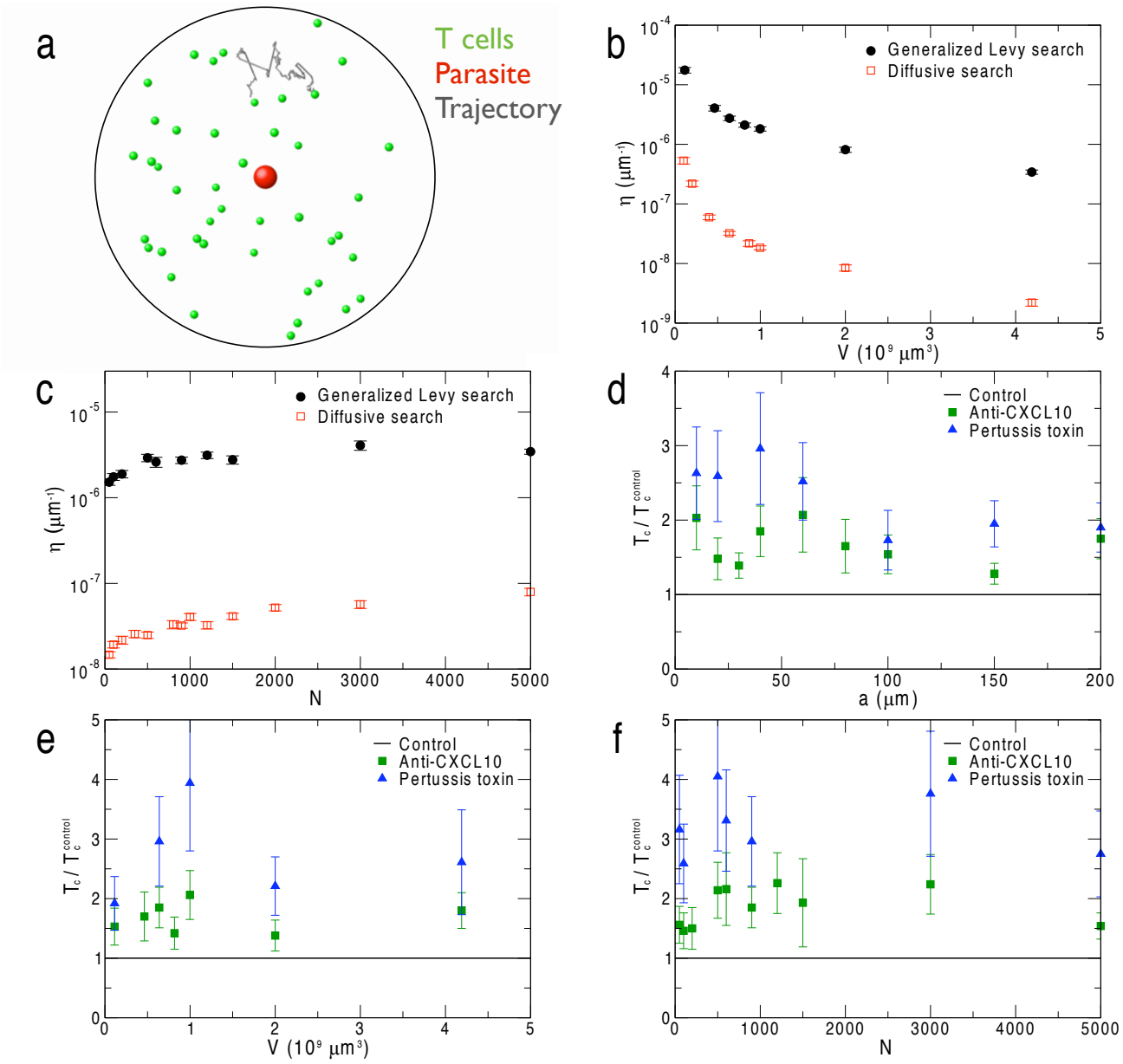

Supplementary Figure 9: The generalized Lévy search is more efficient than a diffusive search, and the chemokine CXCL10 enhances encounter rate in our model. a, To simulate the process of search and capture, we place N walkers (green) in a sphere of volume V with a target of radius a (red) at the origin. A partial sample trajectory is shown in black. **b**, Efficiency, η, for generalized Lévy walkers (black circles) and Brownian walkers (open red squares) as a function of the search volume, V. Generalized Lévy walkers are more efficient in finding the target than Brownian walkers, especially when V is large. **c**, Efficiency for generalized Lévy walkers (black circles) and Brownian walkers (open red squares) as a function of the number of walkers, N. Once again, generalized Lévy walkers are more efficient than Brownian walkers. Additionally, η is insensitive to N above the predicted biological range. **d-f,** We plot the ratio, T_c/T_c^{control}, of time to capture, T_c, to time to capture in control conditions, T_c^{control} for control (black line), anti-CXCL10-treated (green squares), and pertussis-toxin-treated systems (blue triangles). In our model, in all cases studied, cells in control systems located targets the most rapidly, while T cells in pertussis-toxin-treated systems took the longest time to find targets. In the regime of interest, cells in the control found the target in a factor of 1.9 less time than T cells in the anti-CXCL10-treated system and in a factor of 3.0 less time than it took for T cells in pertussis-toxin-treated systems to find the target. Ratios of times to capture are shown over a range of target radii, a (**d**), search volumes, V (**e**), and numbers of searchers, N (**f**).

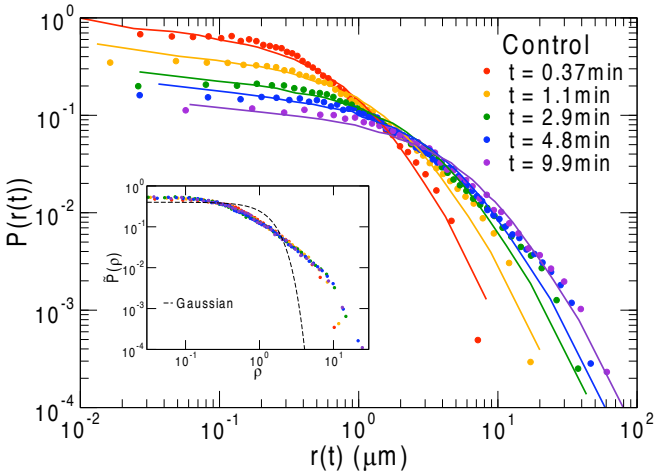

Supplementary Figure 10: The shape of the displacement probability distribution is insensitive to the number of data points per bin. Histograms are generated by binning a fixed number of displacements points in each bin. Here we show that the shape of the distribution remains unchanged by using a smaller number of data points per bin as compared to Fig. 3b in the main text. Here we plot histograms with 1500, 1300, 1000, 650, and 400 displacements per bin for $t = 0.37, 1.1, 2.9, 4.8$, and 9.9 min, respectively. **Inset:** Probability distributions, $\tilde{P}(\rho)$, of rescaled displacements, ρ, at various times still collapse onto a single curve (colored circles).

Supplementary Tables

Model	Akaike Weight
Generalized Lévy walk	1
Stretched exponential distribution	$< 10^{-9}$
Lévy walk with exponentially distributed velocity	$< 10^{-9}$
Lévy walk with slow short flights	$< 10^{-9}$
Pure Lévy distribution	$< 10^{-9}$
Lévy walk with pauses proportional to flight length	$< 10^{-9}$
Gaussian distribution	$< 10^{-9}$
Bimodal correlated random walk	$< 10^{-9}$
Exponential Brownian walk	$< 10^{-9}$

Supplementary Table 1: Akaike weights support the generalized Lévy walk model over other tested models. Models for T cell migration and their respective Akaike weights are listed in order of greatest weight to least weight. All Akaike weights except for that of the generalized Lévy walk are smaller than 10^{-9}, and therefore are effectively zero. Models are described in detail in the Supplementary Discussion subsection "Testing walk models."

μ	μ_{ml}	μ_{bf}		
		500 pts/bin	1000 pts/bin	2000 pts/bin
2.00	2.00	2.03	2.03	2.03
2.50	2.50	2.46	2.46	2.44
3.00	3.00	3.01	2.99	2.95

Supplementary Table 2: The Lévy exponent found from histograms with bins of equal numbers of data points agrees well with the Lévy exponent found using maximum likelihood estimation. As described in the Supplementary Discussion subsection "Testing walk models," we generated 20,000 data points from a Lévy distribution with exponent μ and constructed histograms. We constructed histograms with 500 points per bin, 1000 points per bin, and 2000 points per bin. For each histogram, we used a standard curve fitting routine to find the best-fit Lévy exponent, μ_{bf}. The values of μ_{bf} agree well with the Lévy exponents, μ_{ml} obtained from maximum likelihood estimation.

				500 pts/bin		1000 pts/bin		2000 pts/bin	
μ	ζ	μ_{ml}	ζ_{ml}	μ_{bf}	ζ_{bf}	μ_{bf}	ζ_{bf}	μ_{bf}	ζ_{bf}
2.00	1.00	2.00	1.00	2.04	0.99	2.03	1.00	2.03	1.00
2.50	1.00	2.50	1.00	2.47	0.99	2.46	0.99	2.45	0.99
3.00	1.00	3.00	1.00	3.00	0.99	2.99	0.99	2.94	0.99

Supplementary Table 3: Our binning method is accurate for measuring the Lévy exponent, μ, and scale factor, ζ, simultaneously. Here, the curve fitting routine finds the best-fit scale factor, ζ_{bf}, in addition to the best-fit Lévy exponent, μ_{bf}. For histograms with bins of various sizes, μ_{bf} and μ_{ml}, as well as ζ_{bf} and ζ_{ml} are in close agreement.

Supplementary Discussion

Additional comparisons between model and experimental data

Analysis of directionality

At the outset of the analysis, we looked for directional migration of the T cells. The simplest measure is the mean velocity (the total displacement, which can be positive or negative, over some time interval divided by the time interval). We found that the mean velocity is approximately the size of the error in the measurement and less than 2μm/min, so that the mean drift is practically zero.[21,34–36]

In addition, we calculated the nematic order parameter, S, for the displacement of each cell for each time step:[37]

$$S = \frac{1}{2}\langle 3(\hat{r}_i \cdot \hat{n})^2 - 1\rangle \tag{1}$$

where $\hat{r}_i$ is a unit vector in the direction of a cell displacement and $\hat{n}$ is the director, which specifies the preferred direction of cell displacements. In order to carry out this calculation, we assumed that the director, $\hat{n}$, lay in the direction of the overall drift, and was given by the unit vector in the direction of the mean displacement vector of all cell tracks. The resultant values of S for each experiment were small so that as before, we found no sign of orientational order in the displacements when averaged over all cells and time steps.

Furthermore, we calculated the moment of inertia tensor, I, for each cell trajectory:[38]

$$I = \begin{pmatrix} I_{xx} & I_{xy} & I_{xz} \\ I_{yx} & I_{yy} & I_{yz} \\ I_{zx} & I_{zy} & I_{zz} \end{pmatrix} \tag{2}$$

$$I_{xx} = \sum_i^N (y_i^2 + z_i^2) \tag{3}$$

$$I_{xy} = I_{yx} = -\sum_i^N x_i y_i \tag{4}$$

$$I_{xz} = I_{zx} = -\sum_i^N x_i z_i \tag{5}$$

$$I_{yy} = \sum_i^N (x_i^2 + z_i^2) \tag{6}$$

$$I_{yz} = -\sum_i^N y_i z_i \tag{7}$$

$$I_{zz} = \sum_i^N (x_i^2 + y_i^2) \tag{8}$$

where N is the number of steps in the trajectory and x_i, y_i, and z_i are the x-, y-, and z-components of the i^{th} displacement vector, $\vec{r}_i$. In order to determine whether the cells prefer to move along a particular spatial axis (x, y, z, or some combination of the three), we computed the eigenvalues of the mean moment of inertia tensor, $\langle I\rangle$. We found that on average, the shape of each trajectory is isotropic (uniform) in the x and y directions, but somewhat compressed in the z-direction, as expected for multi-photon imaging where the z-depth is limited by several factors, including the speed of image acquisition. We recalculated the displacement probability distributions taking into account only the components of the displacement in the xy plane; the shapes of the distributions shifted slightly, so that the tails were slightly heavier, but this does not change any of the overall conclusions.

However, these measures do not rule out directional migration. For example, quantities such as the nematic order parameter or the moment-of-inertia tensor, which average over all the trajectories, would not be able to distinguish between randomly-directed migration and directed migration of all cells towards the center of the field of view. Moreover, because our trajectories are necessarily short due to limitations imposed by the size of the field of view, each individual trajectory is anisotropic even though the trajectories are on average isotropic (see, for example, Supplementary Fig. 6). To distinguish whether the anisotropy of individual tracks is due to short-time directional correlations that would disappear if we had longer tracks, or whether it is indicative of directional motion, we carried out the following analysis.

We have quantitatively compared the anisotropies of individual T cell motions to those of individual generalized Lévy walkers taken over the same time interval of 10 min. Note that there is no directional migration in the simulation

model, so that while the model trajectories are anisotropic at short times, they are all isotropic at sufficiently long time scales. To look for evidence of directional migration in the experiment, we computed the two dimensional (xy) moment of inertia tensor for each cell trajectory and determined its eigenvalues. We then calculated the analogous quantities within a simulation of the generalized Lévy walk model obtained by fits to the displacement probability distributions.

For experimental trajectories, we measure averages of $\bar{\lambda}_1 = 195.2 \pm 19.3$ μm^2 and $\bar{\lambda}_2 = 16.5 \pm 1.7$ μm^2. For generalized Lévy walk trajectories, we find comparable averages of $\bar{\lambda}_1 = 178.4 \pm 10.7$ μm^2 and 4.5 ± 0.3 μm^2. Furthermore, as shown in Supplementary Fig. 3, the experimental and model distributions of eigenvalues are quite similar.

The relative magnitudes of the two eigenvalues provide information about the anisotropy of the track. Directional migration would elongate the track and increase the ratio of the larger eigenvalue to the smaller one, compared to the isotropic case. The generalized Lévy walk model does not have an intrinsic directional bias. If directional migration occurs in the experiment, we would therefore expect it to be reflected in a value of the eigenvalue ratio that is larger than in the simulation. Instead, we find that the statistical properties of the two-dimensional moment of inertia of the experimental trajectories are similar in magnitude to those of generalized Lévy walk model (see Supplementary Table 2) and that the ratio of the eigenvalues is actually somewhat smaller in the experiment than in the simulation. These results imply that the anisotropy in the two eigenvalues is due to short-time directional correlations in the trajectories and not to directed migration. We therefore conclude that there is no evidence of directed migration in our experiment. It is possible that there is chemotactic motion on shorter time and length scales and that the motion we analyze is a result of this chemotaxis. However, we cannot resolve it directly with the available data.

Analysis of T cells in anti-CXCL10- and pertussis-toxin-treated mice

In order to determine whether CD8$^+$ T cells in mice treated with anti-CXCL10 antibodies or pertussis toxin also perform generalized Lévy walks, we have plotted the displacement probability distributions, $P(r(t))$, and rescaled displacement distributions, $\tilde{P}(\rho)$ (Supplementary Fig. 8d-e). The displacement distributions reveal that the signals from chemokines and Gα_i-coupled receptors do not affect the character of T cell motility. The shapes of the displacement distributions of CD8$^+$ T cells from anti-CXCL10- and pertussis-toxin-treated mice are independent of time; furthermore, this shape is the same as that found in the control situation.

As an additional comparison between the generalized Lévy walk model and the experiment, we visualized cell tracks in 2D and 3D for the generalized Lévy walk model (Supplementary Fig. 6). We find that these images show qualitative agreement with the corresponding experimental tracks, shown in the main text (Fig. 2e-g, i-k). As in the experiment, walkers in anti-CXCL10- and pertussis-toxin-treated mice in the generalized Lévy walk model exhibit decreased motility compared to the control situation.

Analysis of polyclonal CD8$^+$ T cells, non-antigen-specific CD8$^+$ T cells, and OT-I cells in live mice

To strengthen the evidence for generalized Lévy walks as a typical mode of migration for CD8$^+$ T cells, we examined the displacement distributions of polyclonal T cells, which are specific for multiple different antigens. In Supplementary Fig. 8a, we show that the shapes of the probability distributions are once again independent of time and can be collapsed (inset to Supplementary Fig. 8a) by scaling by a time-dependent scaling factor, $\zeta(t)$. Additionally, we find that polyclonal T cells exhibit displacement correlations that decay slower than exponentially.

To confirm that the observed behavior is not effected by tissue explantation, OT-I cells were imaged through thinned skull of live mice infected with Pru$^{\mathrm{OVA}}$ parasites. We find that the displacement distributions of OT-I cells in live tissue maintain a consistent shape as time progresses (Supplementary Fig. 8b) and can be rescaled by a scale factor, $\zeta(t)$, onto a single broad, non-Gaussian curve (inset to Supplementary Fig. 8b). Consistent with the behavior of generalized Lévy walk, these cells also exhibit long-lived displacement correlations.

Early MP imaging studies demonstrated that T lymphocytes pause in association with antigen presenting cells bearing cognate antigen during priming, with short-term interactions occurring during later stages of priming. To determine whether the presence of cognate antigen within the brain affects generalized Lévy walk behavior, in vitro activated OT-I$^{\mathrm{GFP}}$ and DsRed-expressing P14 cells (specific for ovalbumin and the gp33 protein of LCMV, respectively) were mixed in a 1:1 ratio and transferred into mice infected with Pru$^{\mathrm{OVA}}$ parasites. One day following transfer, each population was equivalent in number and imaged as previously described. At later times post-transfer, the OT-I$^{\mathrm{GFP}}$ population remained abundant, while the P14 cells diminished. Analysis of the cell tracks is presented in Supplementary Fig. 8c and shows that T cell displacement distributions maintain a consistent shape as time progresses, and can be collapsed onto a single, non-Gaussian curve (inset to Supplementary Fig. 8c). Moreover, these cells also exhibit slowly-decaying displacement correlations. Thus, we observe that T cells migrate in a generalized Lévy walk pattern whether or not cognate antigen is present within the brain. These data also suggest that the pausing component of generalized Lévy walk behavior is not caused by antigen recognition.

Together, these data demonstrate that generalized Lévy walk behavior of effector OT-I cells occurs in polyclonal CD8$^+$ T cell populations, occurs in live mice, and is not influenced by the presence of cognate antigen.

Analysis without non-motile cells

One challenge in analyzing the experimental data is the question of how to handle apparently non-motile cells. Several previous studies deem cells moving slower than a certain threshold velocity, typically 2 μm/min, to be stationary.[21,34–36] Such cells are often excluded from the analysis of statistical features such as the MSD.[21] In order to avoid introducing arbitrary cutoffs, we did not exclude non-motile and slow cells from our analysis in the main text.

In order to rule out the presence of artifacts due to non-motile cells, however, we also performed the analysis for the control data set while excluding cells with average speeds of less than 2 μm/min. We find that results of the analysis are insensitive to the inclusion of non-motile cells. Specifically the tails of the probability distributions gain only a small amount of additional weight, the MSD grows with $t^{1.4}$ as in the original analysis, and the displacement correlations are unchanged. We find that the magnitude of the scale factor, ζ, increases significantly. However, we note that the scaling of ζ with time remains unchanged. These results are unsurprising since the non-motile cell populations that are excluded by a speed cutoff are, on average, slower than the full control population. We emphasize, however, that other statistical properties, such as shape of the probability distributions and scaling of the mean squared displacement, remain unchanged.

Model details and additional model results

Simulating and fitting generalized Lévy walks

In the generalized Lévy walk model, a walker moves with fixed speed along a straight path for a distance, ℓ, drawn randomly from a Lévy distribution with Lévy exponent $\mu_{\rm run}$. Once a run is completed, the walker pauses for a time, τ, drawn randomly from a Lévy distribution with Lévy exponent $\mu_{\rm pause}$, before executing another run.

In our simulations of the model, distances, ℓ, or times, τ, are drawn from Lévy distributions with scale factor $\zeta_0 = 1$ (in simulation units, distance ℓ_0 or time t_0) using the method described in ref. 39. Specifically, to obtain a Lévy-distributed random variable, Z_μ, we calculate:

$$Z_\mu = \frac{\sin((\mu-1)X)}{(\cos X)^{1/(\mu-1)}}\left(\frac{\cos((2-\mu)X)}{Y}\right)^{(2-\mu)/(\mu-1)} \tag{9}$$

where X is a uniform random variable on the interval $[-\pi/2, \pi/2]$ and Y has a unit exponential distribution (*e.g.*, Eq. 13; note that Y is generated in the standard way, by calculating $Y = -\ln X'$, where X' is uniform on the interval $[0, 1]$).[39] For runs, once a distance, ℓ is chosen, the walker moves in a randomly chosen direction for a time ℓ/v, where v is the velocity of the walker. For pauses, once a time, τ, is chosen, the walker remains stationary for that amount of time.

In order to fit the generalized Lévy walk model to the experimental data, we must map simulation units onto experimental units. Specifically, we set $200t_0$ equal to 0.37 minutes, the smallest time interval between experimental snapshots, and ℓ_0 equal to 0.091 μm so that we simultaneously match the behavior of the scale factor, $\zeta(t)$, of the walker displacement distribution and the MSD. The choice of $200t_0$ was made in order to ensure that the statistics are good enough to obtain reliable displacement distributions. We have verified that changing the time unit conversion (in conjunction with the length unit conversion) does not significantly alter the agreement between the simulated model and the experiment.

In order to fit the model to data sets of $CD8^+$ T cells in mice treated with anti-CXCL10 antibodies or pertussis toxin, we had a choice of modifying several parameters including the Lévy exponent $\mu_{\rm run}$ and $\mu_{\rm pause}$, the typical time scale of a pause (the pausing scale factor), the conversion of simulation length units, ℓ_0, and time units, t_0, the walker instantaneous velocity, v (in units of $v_0 = \ell_0/t_0$), and various combinations.

We find that while holding $\mu_{\rm run}$ and $\mu_{\rm pause}$, as well as the instantaneous velocity, v, during runs fixed, we can fit the anti-CXCL10 and pertussis-toxin data by increasing the typical pause time. For instance, with $\ell_0 = 0.091$ μm, T cells in anti-CXCL10- and pertussis-toxin-treated mice are reasonably well-described by a generalized Lévy walk with the same typical run lengths and instantaneous walker velocities, but with pauses that are 2 and 4 times longer, respectively.

As described in the main text, we also find that by scaling the simulation length, ℓ_0, alone, we can capture the behavior of cells in anti-CXCL10- and pertussis-toxin-treated mice. In particular, cells in anti-CXCL10-treated mice, $\ell_0 = 0.067$ μm, and for pertussis-toxin-treated mice, $\ell_0 = 0.049$ μm.

Thus, cells in anti-CXCL10- and pertussis-toxin-treated mice can be described with the same Lévy distributions for runs and pauses but with (1) a smaller instantaneous velocity and shorter typical run length or (2) longer pause durations.

We note that we do not directly control the average walker velocities in our models. Instead, we vary the simulation unit, v_0, of instantaneous velocity (by varying ℓ_0) during runs to fit the data. However, upon performing this procedure, we find that the resulting simulated average track velocity is in reasonable agreement with the experimental data.

Search and capture

To model the process of search and capture, we wrote a C++ simulation in which we placed N walkers in a sphere of volume V with a target of radius a at the origin (Supplementary Fig. 9a).[40,41] We estimated N, V, and a as follows. From flow cytometry, we estimated that there are 300,000-450,000 T cells and 300-500 parasites/cysts in the brain. The T cells explore a volume of at most 3.2-4.4 $\times 10^{11} \mu$m^3. Parasites/cysts and T cells have radii of 5-10 μm. Detection may occur upon contact, or perhaps within a short distance of contact. Thus, we estimated that the effective target radius for point-sized random walkers is 10-50 μm.

For our model, there is one cyst per sphere, so there are 600-1500 T cells within the sphere and the sphere volume of 6.4×10^8 to $1.5 \times 10^9 \mu$m^3. Our standard choice is $N = 900$, $V = 6.4 \times 10^8 \mu$m^3 and $a = 40 \mu$m. In Supplementary Fig. 9b, we plot the efficiency (defined in the main text and refs. 28 and 42) for the generalized Lévy walkers and for random walkers as a function of the volume V of the sphere. As expected, the efficiency decreases with increasing sphere volume. In Supplementary Fig. 9c we plot it as a function the number of T cells, N, in the sphere. The capture time is estimated to be of order 200 min in our simulations; thus, the discrepancy between the time scale over which we are able to observe T cell tracks and the relevant time scale for the immune response may be small. Additionally, we note that the efficiency depends only weakly on N for $N > 1000$. Thus, the physiological numbers for N appear to be near the minimum needed to achieve a high efficiency.

We have also calculated the time for each walker to reach the target, and have averaged over walkers to obtain the capture time. These calculations were carried out for generalized Lévy walkers in the control, anti-CXCL10- and pertussin-toxin treated mice. The ratio of capture time for cells in anti-CXCL10- and pertussin-toxin treated mice to the capture time of cells in the control mice is shown in Supplementary Fig. 9d-f as a function of (d) target radius a, (e) search volume V and (f) number of walkers, N. As expected, the capture time is higher for cells in mice treated with anti-CXCL10 or pertussis-toxin than for control cells, implying that the chemokine shortens the capture time.

We note that although generalized Lévy walkers are clearly more efficient in locating targets than Brownian walkers, the determination of the optimal search strategy remains an open question. The optimality of a search strategy may depend on a variety of system-specific factors, such as the ability of the searchers to adapt to their environment, efficiently and accurately detect their targets, and reliably capture their targets once detected.[29,43] Moreover, it is unclear whether efficiency in terms of targets located per distance traveled is truly the best measure of T cell capability. Consequently, there may be a variety of other ways in which generalized Lévy walks benefit T cells.

Generalized Lévy walks vs. other types of walks

Various models have been proposed for cell migration.[20,41,44–46] Here we discuss the evidence that the generalized Lévy walk is a better model for CD8$^+$ T cell migration in the brain than models that are commonly found in the literature.

As discussed in the text, we looked at several measures of the migration tracks to gain a more complete view of the walk statistics. In particular, we evaluated the (1) mean-squared displacement, (2) the distribution of displacements, not just at a single time but as a function of time, (3) the scale factor used to collapse the displacement distribution, and (4) the displacement correlation function in time.

Our experimentally observed walks are clearly inconsistent with random walks.[41] For random walks, the displacement distribution is Gaussian at all times, in clear contrast with the shape we observe (see Fig. 3b). We note that if our tracks were describable by persistent random walks, the shape of the displacement distribution would evolve in time, finally approaching a Gaussian shape at long times. This is inconsistent with our data.

For a random walk, the scale factor for collapsing the distribution, $\zeta(t)$, is identical to the root-mean-squared displacement for a random walk. For a persistent random walk, $\zeta(t)$ approaches the root-mean-squared displacement at long times. Supplementary Fig. 4 shows that these two quantities do not coincide for our walks, and do not converge at long times. Finally, the displacement correlations should decay exponentially with time for a random walk, in clear contrast to our walks (inset to Fig. 3c). These observations convince us that our data cannot be described by Brownian walks.

The fact that the shape of the displacement distribution in Fig. 3b does not change with time and has a much heavier tail than a Gaussian distribution suggests that the migration tracks might be well described by a Lévy walk.[47,48] Lévy distributions, like Gaussian distributions, are stable in the sense that the sum of a set of Lévy-distributed random variables is also a Lévy distributed random variable. Lévy distributions are asymptotically described by

$$L_\mu(\ell) \sim \ell^{-\mu} \tag{10}$$

where ℓ is a displacement and μ is the "Lévy exponent" and takes on a value $1 < \mu < 3$.

In a Lévy walk, a time, $t(\ell)$, is associated with each step of size ℓ drawn from a Lévy distribution. In the standard model of Lévy walk, the walker moves at fixed speed v so that the duration of a step of size ℓ is $t(\ell) = \ell/v$. In this model, the mean-squared displacement is well-defined, and is typically superdiffusive, so that $\langle r^2 \rangle \sim t^\alpha$, where

$\alpha > 1$.[47,49] The displacement correlation function decays as a power-law with time.[50] In addition, the overall shape of the displacement distributions of Lévy walkers is not Gaussian and is approximately independent of time (see, for example, refs. 22, 51, and 52). Thus, we can once again define a scaling factor, $\zeta(t)$, that can be used to rescale displacements, r, and collapse the probability distributions, $P(r;t)$, onto a single curve.

Such a Lévy walk is also inconsistent with our data, as shown in Supplementary Fig. 4. In Supplementary Fig. 4b, we show that the displacement distributions are reasonably well described by a Lévy walk with $\mu = 1.9$ (although it is systematically too high in the tail of the distribution). However, such a walk would have a scale factor and root-mean-squared displacement that do not agree with our data (Supplementary Fig. 4c). In addition, the expected displacement correlation does not fit our data (inset to Supplementary Fig. 4c). Thus, the $CD8^+$ T cell tracks are not described by fixed-speed Lévy walks.

In contrast, all four statistical measures of T cell migration tracks are consistent with the generalized Lévy walk model[22] (Fig. 3). We note that while our model is constructed from Lévy distributions, it is distinct from the standard Lévy walk. In particular, the probability distributions, scaling factor, and MSD for a given $\mu_{\rm run}$ and $\mu_{\rm pause}$ are, in general, quite different than those quantities resulting from a Lévy walk with $\mu = \mu_{\rm run}$. Despite these significant quantitative differences, however, the generalized Lévy walk model still demonstrates superdiffusive motility, long-time displacement correlations, and approximately stable, non-Gaussian distributions.[22]

Testing walk models

Various methods exist in the literature[23,24,30,50,53–56] for testing whether migration tracks obey Lévy behavior. Below we summarize the results of these methods when applied to our migration data.

Construction of displacement probability distributions

We first note that it is more informative to study the entire shape of the displacement distribution than to focus only on its second moment (the mean-squared displacement). To obtain the distribution, however, it is necessary to generate histograms of binned displacements. In order to improve the statistics, we separated displacements into their x, y, and z components and binned the components. We find that each component is described by the same distribution.

It has been pointed out that the shape of the displacement distribution can be biased by how the data are binned.[30,53,55] In particular, if one uses bins of constant width, the number of counts per bin is much smaller in the tail than near the peak of the distribution, giving rise to larger statistical errors in the tail. Similar bias can be introduced if one uses bins of logarithmically varying width[30,53,55] for a distribution that is not a pure power law.

To avoid this biasing and maintain equal statistical errors in all bins, we binned the data with a constant number of displacement data points per bin. For instance, in Fig. 3b of the main text, for $t = 0.37$ minutes, we placed 2000 displacements into each bin. Thus, we did not directly control the width of each bin; rather, the widths varied according to the experimentally observed distribution of data points. The idea behind this binning method is that the bin locations and widths will be distributed in such a way so that they reproduce the actual shape of the distribution without the biases. We have tested our binning method with test cases of known Lévy distributions and maximum likelihood estimation, similar to what has already been done for linear and logarithmic binning methods in refs. 30 and 55.

To begin, we generated a set of 20,000 data points (approximately equal to the total number of cell displacements in the experiment) from a Lévy distribution with exponent μ. We then put 1000 displacements in each bin and use a standard curve fitting routine to find the "best-fit" $\mu_{\rm bf}$. Then, we performed the maximum likelihood estimation (MLE; described in refs. 23, 54, and 55) to find the "most likely" $\mu_{\rm ml}$. We also used this procedure to verify that our binning method does not have a significant bin size dependence. The results are summarized in the Supplementary Tables 2 and 3. The tables show that the error in our binning method in reproducing the correct value of μ (and ζ) is only a few percent. Thus, this binning method does not suffer from the flaws discussed in refs. 30 and 55 that cause other binning methods to dramatically and systematically underestimate μ.

To further test the accuracy of our results, we repeated this procedure for displacement histograms with various numbers of data points per bin. The shapes of the distributions appear to be independent of the number of data points per bin used to construct the histograms, giving confidence in the reliability of the distributions we obtained (compare, *e.g.*, Supplementary Fig. 10 and Fig. 3b in the main text).

Instead of looking at the displacement distributions, one can plot the survival frequency, $S(r)$, which is given by one minus the cumulative distribution.[30,53,55] At a given displacement, r, the survival frequency is the total probability weight $r' > r$ and is given by:

$$S(r) = 1 - \int_0^r P(r')\mathrm{d}r' = \int_r^\infty P(r')\mathrm{d}r' \tag{11}$$

Typically, the survival frequency is used to identify features in the tail (large displacements) of the distribution. For instance, in a standard Lévy walk, $S(r)$ should decay as a power law at large displacements.[30,53,55,57] The drawback

of the survival frequency, as refs. 58 and 59 note, is that this quantity is extremely sensitive to the shape of the tail of the distribution. Because there is necessarily less data in the tail, it is the noisiest part of the distribution, and so small statistical differences can be amplified in the survival frequency. Furthermore, for any physical system, there is necessarily some influence of truncation effects, such as finite limits to pause times and run lengths, and experimental artifacts such as a finite field of view.[58–60] Although we have numerically modeled generalized Lévy walkers in a finite-sized field of view, the full impact of truncation is unclear. We therefore focus on the entire shape of the distribution, rather than on the survival frequency.

Maximum likelihood estimation

Another method that is used to examine migration data is maximum likelihood estimation (MLE).[23,54,55] This method involves testing specific functional forms of the displacement distribution and determining which function is most likely to describe the data. Typically, MLE is computed for displacements over a single time interval; in contrast, we computed the most likely values of μ_{run} and μ_{pause} given the cell displacements over all measured time intervals in order to more accurately determine the most likely Lévy exponents. MLE is typically used when the exact analytical form of the model probability distribution is known. Since we do not know the analytical form of the generalized Lévy walk probability distribution, we could only apply this test by interpolating between points in a numerically generated probability distribution. In doing this, we discovered that the combination of μ_{run} and μ_{pause} chosen by the MLE is sensitive to the construction of the histogram of generalized Lévy walker displacements. This problem arises because the probability distributions of some generalized Lévy walks are very similar. Thus, we paid particular attention to minimizing the effects of 1) the noise in each point generated on the histogram resulting from the fact that there are a finite number of displacements per bin, and 2) the error arising from interpolating the value of the probability between neighboring histogram points, arising from the fact that the bins have a nonzero width.

In order to understand how noise affects the MLE, we first chose a number, n, of bins to use to construct displacement histograms (for example, we used 15, 30, and 75 bins). For the chosen number of bins, we constructed histograms with a fixed number, m, of points per bin, as described in the main text, and performed the MLE. We repeated this procedure for various m in order to understand the behavior of the most likely combination of μ_{run} and μ_{pause} in the limit that the uncertainty in each histogram data point becomes small (large m).

In the same spirit, we studied the behavior of the most likely combination of μ_{run} and μ_{pause} in the limit that the error due to interpolating between histogram points becomes small (large n). To do this, we fixed the number, m, of displacements per bin (for example, we tried 1000, 2000, and 5000 displacements per bin), and numerically generated probability distributions for the MLE. We then examined the behavior of the estimate with increasing n.

For both extrapolations, the best μ_{run} lies between 2.1 and 2.2 and the best μ_{pause} is between 1.6 and 1.7. In order to select a precise combination, we compared the correlation function, $K(\tau, t)$, of the generalized Lévy walk to the experimental data. We found that a generalized Lévy walk with $\mu_{\text{run}} = 2.15$ and $\mu_{\text{pause}} = 1.7$ fits the data very well.

Akaike information criterion

The Akaike information criterion (AIC) quantitatively describes the amount of evidence for a given model. It accounts for both the likelihood (calculated by MLE) and the complexity (number of parameters) of a given model. The AIC is used to calculate the probability of a given model to be the most accurate of all the tested models (the Akaike weight).[24,55]

We are only able to identify a few candidate models with probability distributions that resemble those of the experimental data. Furthermore, only certain types of models exhibit the observed features, such as the time-independent shape of the displacement probability distributions. Thus, the AIC and Akaike weights are only of limited use in this study. Despite these issues, we have calculated the Akaike weights for various possible models using the probability distributions, $P(r(t))$, at $t = 0.37$ min.

We consider the generalized Lévy walk, a Lévy flight, Lévy walks with runs of duration $t \propto r^{-\nu}$, a Lévy walk alternating with pauses that are run-length-dependent, a stretched exponential distribution, a Brownian walk with exponentially-distributed runs (described below), and the bimodal correlated random walk (described below and in refs. 25 and 61). For other models, MLE does not converge to a meaningful result, so the Akaike weight cannot be calculated. As expected, the Akaike weight is highest for the generalized Lévy walk; indeed, none of the other models tested have a significant Akaike weight (the stretched exponential distribution had the second highest Akaike weight, but was still less than 10^{-9} (Supplementary Table 1).

Other models of cell migration

It has recently been proposed that populations of walkers that have varied characteristics can produce apparent collective Lévy behavior and power-law statistics even if the behavior of each individual walker is not Lévy-like.[56] This is an important distinction because it can mean that walkers individually move in a diffusive (random-walk

like) manner even though the collective motility appears to be superdiffusive. For example, consider a population composed of N walkers, indexed by i, that execute straight runs for a distance, ℓ, drawn from an exponential distribution,

$$E(\ell;\lambda_i) = \frac{1}{\lambda_i} \mathrm{e}^{-\ell/\lambda_i}. \tag{12}$$

If the set of decay lengths, λ_i, of the population varies sufficiently, the statistical properties of the entire population can collectively appear to exhibit Lévy characteristics.[56]

In order to identify whether migrating populations truly perform generalized Lévy walks or simply have a large amount of variation between individuals, we rescale the displacements, $r(t)$, between two times, τ and $\tau + t$, of each individual walker by the walker's mean displacement, $\langle |r(t)| \rangle$, as suggested in ref. 56. If the resulting probability distribution, $P^*(\kappa(t))$, of rescaled displacements, $\kappa(t)$, falls on a unit exponential distribution,

$$E(\kappa(t);1) = \mathrm{e}^{-\kappa(t)}, \tag{13}$$

the collective behavior may be attributable to variation within a population of walkers that run for exponentially-distributed distances.

We find that the distribution, $P^*(\kappa(t))$, of rescaled (x, y, and z components of) displacements, $\kappa(t)$, with $t = 0.37$ min, appear to be distributed as a unit exponential distribution given by Eq. 13 (Supplementary Fig. 5a), possibly indicating the behavior proposed above. However, we find that this does not hold for larger t (Supplementary Fig. 5a), and moreover, distributions of rescaled displacements at larger t do not appear to decay strictly exponentially (inset to Supplementary Fig. 5a). Thus, the apparent exponential behavior appears to be incidental rather than universal, which suggests that the exponential model does not accurately describe the data. Moreover, we find that when we rescale the full displacements, $r = \sqrt{x^2 + y^2 + z^2}$, the data fail to collapse onto an exponential distribution (Supplementary Figs. 5b-c). This implies that the Lévy-like characteristics that we see do not result from variation between different random walkers, but from deviation of each walk from a random-walk model.

As another test of this result, we simulated walkers executing runs from exponential distributions with mean run lengths taken from the set of experimentally observed run lengths. In all cases, we find that the model with walkers making exponentially distributed runs cannot reproduce the observed behavior of T cells, even when variation in the mean run length is included. For example, Supplementary Figs. 5b-c show that the displacement probability distributions of walkers in the exponential model are markedly different than our experimental observations. Once again, this suggests that an exponential-type model cannot account for the Lévy-like characteristics we observe in T cell migration.

Another model that has recently been proposed for intermittent migration is the bimodal correlated random walk (BCRW) model.[25,61] The BCRW model is composed of two alternating correlated random walks, one in which the walker moves in exponentially-distributed, directed flights, and another in which the walker takes short, randomly-oriented steps as it reorients for an exponentially-distributed time. Thus, as described by refs. 25 and 61, the BCRW model may yield superdiffusion at short times, but must yield diffusive behavior (with Gaussian distributions) at long times.

In order to determine whether the BCRW model can explain the experimental data we performed the bimodal analysis described in refs. 25 and 61. Briefly, the bimodal analysis marks the beginning of directional walk modes when the angles, θ_i, θ_{i+1}, and θ_{i+2}, between four successive cell displacement vectors ($\vec{r}_i, \vec{r}_{i+1}, \vec{r}_{i+2}$, and $\vec{r}_{i+3}$) fall below some threshold angle, θ'. Reorientation modes begin if θ_i and θ_{i+1} exceed θ', or if $\theta_i > \theta'$ and the angle, ϕ_{i+2}, between the vectors $\vec{s}_i = (\vec{r}_{i-1} + \vec{r}_i)$ and $\vec{s}_{i+2} = (\vec{r}_{i+1} + \vec{r}_{i+2})$ is greater than θ'. We performed this analysis for various values of threshold angle θ'. In all cases, we find that the bimodal analysis frequently failed to detect the onset of directional motion; an example of a directed flight not detected by the bimodal analysis is shown in Supplementary Fig. 5d.

We also directly compare the BCRW model to the experimental data by simulating a system of walkers executing bimodal correlated random walks. We simulated BCRWs constructed with the mean step and flight lengths measured by the bimodal analysis of the T cell migration data. For various θ', the system of bimodal correlated random walkers does not generate statistics matching the experimental data. For example, in Supplementary Fig. 5e, we show that the displacement probability distributions of the BCRW model are clearly different than what we experimentally observe. Furthermore, the BCRW probability distributions do not collapse onto a single curve, and they systematically shift toward a Gaussian distribution as time progresses (inset to Supplementary Fig. 5e). Taken together, the bimodal analysis and BCRW simulations demonstrate that $CD8^+$ T cells migrate in a way that cannot be described by the bimodal correlated random walk model.

In addition to exponential Brownian and BCRW models, we also considered various other Lévy-walk-related models for cell migration. All of the following models fail to consistently describe all of the statistical properties of the experimental data:

• Standard Lévy walks, composed solely of fixed-velocity straight runs of a Lévy-distributed length (Supplementary Fig. 4).

• Standard Lévy walks with either fixed truncation[60] or an exponentially-decaying tail.[62]

• Lévy walks with a randomly distributed velocity. We tried several different Gaussian, exponential, and Lévy distributions for the velocity.

• Lévy walks where the velocity is proportional to $r^{\nu-1}$, where r is the run length, and ν, in principle, can take on any real value.[49]

• Standard Lévy walks where runs of length $r > r_0$ are traversed at a given fixed velocity and time to complete a run of length $r < r_0$ is given by $t = cr^{-\nu}$, where r_0 is a threshold length and c is some constant ("Lévy walks with slow short flights" in Supplementary Table 1).

• Standard Lévy walks where runs of length $r > r_0$ are executed at a given fixed velocity and the walker pauses whenever a length $r < r_0$ is drawn from the Lévy distribution.

• Lévy-distributed runs alternating with pauses lasting either a fixed amount of time or an exponentially-distributed amount of time.

• Lévy-distributed runs alternating with pauses of duration $t = cr^{-\nu}$, where r is the previous run length and c is a constant ("Lévy walk with pauses proportional to flight length" in Supplementary Table 1).

• Lévy-distributed runs alternating with pauses of duration, $t = Ae^{-cr}$, where r is the previous run length and A and c are constants.

We also examined variations on the generalized Lévy walk model. For example, we considered walkers that alternate Lévy distributed runs with simple random walks instead of pauses, and walkers that have simple random walks overlaying and adding noise to the generalized Lévy walk. These models do not describe the data as well as the basic version of the generalized Lévy model described in the main text.

References

[34] Lindquist, R. L. *et al.* Visualizing dendritic cell networks *in vivo*. *Nature Immunol* **5**, 1243-1250, doi:10.1038/ni1139 (2004).

[35] Ng, L. G. *et al.* Migratory dermal dendritic cells act as rapid sensors of protozoan parasites. *PLoS Pathogens* **4**, e1000222, doi:10.1371/journal.ppat.1000222 (2008).

[36] Deguine, J., Breart, B., Lemaitre, F., Di Santo, J. P. & Bousso, P. Intravital imaging reveals distinct dynamics for natural killer and $CD8^+$ T cells during tumor regression. *Immunity* **33**, 632-644, doi:10.1016/j.immuni.2010.09.016 (2010).

[37] Chakin, P. M. & Lubensky, T. C. *Principles of Condensed Matter Physics*. (Cambridge University Press, Cambridge, 2000).

[38] Taylor, J. R. *Classical Mechanics*. (University Science Books, Sausalito, 2005).

[39] Jacobs, K. *Stochastic processes for physicists: understanding noisy systems*. (Cambridge University Press, Cambridge, 2010).

[40] Berg, H. C. & Purcell, E. M. Physics of chemoreception. *Biophys J* **20**, 193-219 (1977).

[41] Berg, H. C. *Random Walks in Biology*. (Princeton University Press, Princeton, 1993).

[42] Bartumeus, F., Catalan, J., Fulco, U. L., Lyra, M. L. & Viswanathan, G. M. Optimizing the encounter rate in biological interactions: Lvy versus Brownian strategies. *Phys Rev Lett* **88**, 097901 (2002).

[43] Reynolds, A. M. Adaptive Lévy walks can outperform composite Brownian walks in non-destructive random searching scenarios. *Physica A* **388**, 561-564 (2009).

[44] Schuster, F. L. & Levandowsky, M. Chemosensory responses of *Acanthamoeba castellanii*: visual analysis of random movement and responses to chemical signals. *J Euk Microbiol* **43**, 150-158 (1996).

[45] Germain, R. N., Miller, M. J., Dustin, M. L. & Nussenzweig, M. C. Dynamic imaging of the immune system: progress, pitfalls and promise. *Nat Rev Immunol* **6**, 497-507 (2006).

[46] Reynolds, A. M. Can spontaneous cell movements be modelled as Lévy walks? *Physica A* **389**, 273-277 (2010).

[47] Shlesinger, M. F., West, B. J. & Klafter, J. Lévy dynamics of enhanced diffusion: application to turbulence. *Phys Rev Lett* **58**, 1100-3 (1987).

[48] Shlesinger, M. F., Zaslavsky, G. M. & Klafter, J. Strange kinetics. *Nature* **363**, 31-7 (1993).

[49] Blumen, A., Zumofen, G. & Klafter, J. Transport aspects in anomalous diffusion: Lévy walks. *Phys Rev A* **40**, 3964-73 (1989).

[50] Viswanathan, G. M., Raposo, E. P., Bartumeus, F., Catalan, J., & da Luz, M. G. E. Necessary criterion for distinguishing true superdiffusion from correlated random walk processes. *Phys Rev E* **72**, 011111 (2005).

[51] Araujo, M., Havlin, S., Weiss, G. H. & Stanley, H. E. Diffusion of walkers with persistent velocities. *Phys Rev A* **43**, 5207-13 (1991).

[52] Buldyrev, S. V. *et al.* Generalized Lévy-walk model for DNA nucleotide sequences. *Phys Rev E* **47**, 4514-4523 (1993).

[53] Benhamou, S. How many animals really do the Lévy walk? *Ecology* **88**, 1962-9 (2007).

[54] Edwards, A. M. et al. Revisiting Lévy flight search patterns of wandering albatrosses, bumblebees and deer. *Nature* **449**, 1044-8 (2007).

[55] Edwards, A. M. Using likelihood to test for Lévy flight search patterns and for general power-law distributions in nature. *J Anim Ecol* **77**, 1212-22 (2008).

[56] Petrovskii, S., Mashanova, A., & Jansen, V. A. A. Variation in individual walking behavior creates the impression of a Lévy flight. *Proc Natl Acad Sci U S A* **108**, 8704-7 (2011).

[57] Zumofen, G., Klafter, J., & Blumen, A. Anomalous transport: a one-dimensional stochastic model. *Chem Phys* **146**, 433-444 (1990).

[58] Boyer, D., Miramontes, O. & Ramos-Fernández, G. Evidence for biological Lévy flights stands. *Arxiv* http://arxiv.org/abs/0802.1762 (2008).

[59] Viswanathan, G. M., Raposo, E. P. & da Luz, M. G. E. Lévy flights and superdiffusion in the context of biological encounters and random searches. *Phys Life Rev* **5**, 133-150 (2008).

[60] Mantegna, R. N. & Stanley, H. E. Stochastic process with ultraslow convergence to a Gaussian: the truncated Lévy flight. *Phys Rev Lett* **73**, 2946-2949 (1994).

[61] Potdar, A. A., Jeon, J., Weaver, A. M., Quaranta, V. & Cummings, P. T. Human mammary cells exhibit a bimodal correlated random walk pattern. *PLoS One* **5**, e9636 (2010).

[62] Koponen, I. Analytic approach to the problem of convergence of truncated Lévy flights towards the Gaussian stochastic process. *Phys Rev E* **52**, 1197-1199 (1995).

Movie Legends

Supplementary Movie 1. OT-I$^{\mathbf{GFP}}$ migration in the brains of control mice. OT-I$^{\mathrm{GFP}}$ cells (green) and secondary harmonic signal (blue) were imaged in explant brain of control mice. Images were acquired in 3 dimensions over a total of 10 minutes.

Supplementary Movie 2. OT-I$^{\mathbf{GFP}}$ migration in the brains of anti-CXCL10-treated mice. OT-I$^{\mathrm{GFP}}$ cells (green) and secondary harmonic signal (blue) were imaged in explant brain of mice treated with anti-CXCL10 antibody. Images were acquired in 3 dimensions for a total of 10 minutes.

Supplementary Movie 3. OT-I$^{\mathbf{GFP}}$ migration in the brains of pertussis-toxin-treated mice. OT-I$^{\mathrm{GFP}}$ cells (green) and secondary harmonic signal (blue) were imaged in explant brain of mice treated with pertussis toxin. Images were acquired in 3 dimensions over a total of 10 minutes.